Eur. Phys. J. A (2016) **52**: 148
DOI 10.1140/epja/i2016-16148-4

THE EUROPEAN PHYSICAL JOURNAL A

Regular Article – Experimental Physics

The neutron cross-section functions for the reactions ^{187}Re(n, α)^{184}Ta, ^{187}Re(n, 2n)^{186}Re and ^{185}Re(n, 2n)^{184}Re in the energy range 13.08–19.5 MeV

N. Jovančević[1,2], L. Daraban[1], H. Stroh[1], S. Oberstedt[1,a], M. Hult[1], C. Bonaldi[1], W. Geerts[1], F.-J. Hambsch[1], G. Lutter[1], G. Marissens[1], and M. Vidali[1]

[1] European Commission, Joint Research Centre, Institute for Reference Materials and Measurements (IRMM), Retieseweg 111, 2440 Geel, Belgium
[2] Department of Physics, Faculty of Sciences, University of Novi Sad, Trg Dositeja Obradovica 3, 21000 Novi Sad, Serbia

Received: 2 March 2016 / Revised: 5 April 2016
Published online: 31 May 2016

Communicated by P. Woods

Abstract. In the present work, measurements of the cross-section functions for the ^{187}Re(n, α)^{184}Ta, ^{187}Re(n, 2n)^{186}Re and ^{185}Re(n, 2n)^{184}Re reactions were performed in the energy range 13.08–19.5 MeV. We applied the neutron activation technique using several wide-energy neutron beams (NAXSUN), recently developed at the JRC-IRMM. This method involves measuring the activity of the radionuclides produced in a target by the in energy overlapping neutron beams and a subsequent unfolding procedure. The present results are the first experimental data on these cross-sections for incident neutron energies between 15 and 19.5 MeV and may contribute to improving evaluations and nuclear models.

1 Introduction

Elemental rhenium consists of a pair of stable isotopes, ^{185}Re (37.4%) and ^{187}Re (62.6%). The metal is a high-temperature corrosion resistant material. Therefore, it first found applications in jet-engines for the airplane industry and later for special uses, such as in nuclear power-sources for space applications [1]. Also, rhenium and its alloys with boron are known as effective neutron absorbers for the regulation of nuclear reactors [2] but up to now, rhenium has not generally been used in conventional fission reactors. However, rhenium with its high-temperature resistance is an interesting material for the construction of nuclear reactors, and this explains the interest for new measurements of neutron interaction cross-sections with this element.

Two Re radionuclides have found applications in the medical field. ^{186}Re and ^{188}Re are used for cancer treatment/diagnostics [3–6]. Rhenium can also be used as target for production of tantalum and tungsten radionuclides [7]. For all possible use of Re for nuclear technology and in medical applications, it is of high interest to have accurate cross-section data for the nuclear reactions on rhenium and especially neutron activation reactions. Moreover, the data is also needed for fundamental research in astrophysics and, in particular, to gain a better understanding of the stellar nuclear synthesis via the Re/Os cosmos-chronometry [8].

However, an overview of the existing experimental results shows a severe lack of satisfactory data for the neutron excitation cross-section values [9]. At low energies, only neutron capture information is available [10]. Rhenium elastic and inelastic scattering cross-sections at incident energies of less than 1.5 MeV were reported in [11]. Since then, a number of additional measurements employed the time-of-flight technique [12].

Thus, in this work measurements of the neutron cross-section values for the ^{187}Re(n, α)^{184}Ta, ^{187}Re(n, 2n)^{186}Re and ^{185}Re(n, 2n)^{184}Re reactions have been performed in the energy range 13.08–19.5 MeV. We present here results for the excitation functions for the reactions to the ground state in ^{184}Ta, ^{187}Re and ^{186}Re nuclei. Results on the population of the long-lived isomeric state in ^{184m}Re and ^{186m}Re will be the subject of a forthcoming study. The available experimental data show that only few measurements were carried out in the past, all but one in the neutron energy range between 13 MeV and 15 MeV [13–15]. In this work, the technique of measuring the neutron activation cross-section using wide-energy neutron beams (NAXSUN, Neutron Activation X-Section determined using UNfolding), developed at JRC-IRMM, was

[a] e-mail: Stephan.OBERSTEDT@ec.europa.eu

employed [15–17]. This technique allows obtaining a cross-section function in a wide energy range, which is different from the usual point-wise data measured at well-defined incident neutron energies.

2 The NAXSUN method

The technique for measuring the neutron activation cross-section using wide-energy neutron beams involves the following steps:

i) Irradiation of several (6 in this study) pure metal disks in different wide-energy neutron beams that overlap with each other. Only one disk is irradiated in each beam.

ii) To obtain an absolute value of the cross-section (and thereby normalising the obtained excitation function) one further disk, irradiated at a well-defined incident neutron energy, was measured.

iii) Gamma-ray spectrometry of each disk to determine the activity of the produced radionuclides.

iv) Calculation of the neutron cross-section function using an unfolding procedure, where the known spectra of the neutron beams and the activity of the radionuclides are input parameters.

This method was first tested on the well-known neutron excitation function of the reactions $^{113}\mathrm{In}(\mathrm{n},\mathrm{n}')^{113\mathrm{m}}\mathrm{In}$ and $^{115}\mathrm{In}(\mathrm{n},\mathrm{n}')^{115\mathrm{m}}\mathrm{In}$. The next development was to introduce a new procedure to determine the default function for the unfolding technique [16]. That function is basically the starting point for the iterative unfolding procedure. The NAXSUN technique, like any other activation technique, relies on a careful monitoring of the neutron fluence during irradiation, but does not require *a priori* knowledge about the investigated excitation function.

As is described in ref. [17], the NAXSUN technique involves the measurement of the induced specific activity per atom of a radionuclide of interest, A_k, in disk "k", which is proportional to the product of the cross-section for a certain reaction and the corresponding neutron fluence rate:

$$A_k = \sum_i \Phi_{ki} \cdot \sigma_i; \quad i = 1, 2, \ldots, c; \quad k = 1, 2, \ldots, m, \tag{1}$$

where Φ_{ki} are the values of neutron fluxes for a certain energy bin, E_i, in the case of the irradiation of disk k. In eq. (1) σ_i denotes the values of the neutron excitation function, which correspond to the energy E_i. The index k runs over the number of irradiated disks, and m is the number of disks. The maximum value for the index I, c, denotes the number of bins in the neutron spectra and the excitation function curve. All disks were of identical size and weight. This is not a pre-requisite of the method, but simplifies the data analysis (*e.g.*, determination of neutron flux at disk position, gamma detector efficiency) and also provides the cross-section data as measured under the same conditions.

Table 1. Mass values of the metallic rhenium disks used for the activation.

Disk No.	Mass (g)
1	28.93180(5)
2	30.13020(5)
3	29.83400(5)
4	29.77400(5)
5	30.25310(5)
6	29.01820(5)
7	30.23730(5)

The above system of equations (1) is underdetermined and possesses an infinite number of solutions. Hence, for the determination of the cross-section values it is necessary to use an unfolding procedure. In this work we used again the MAXED and GRAVEL algorithms [15,16,18,19]. The unfolding procedures require an initial guess function that can be chosen based on some *a priori* information, *i.e.* the corresponding evaluated activation cross-section data file or from other existing experimental data [13,14]. It is important that the chosen default excitation function is similar to the experimental data. This is solved by performing linear interpolation of the average value of the cross-section for each irradiation and different neutron fields [16,17]. In this work, also one point-wise measurement was performed at a well-defined energy and the data was used for normalizing the obtained neutron excitation cross-section functions.

It must be mentioned here that the NAXSUN technique cannot provide cross-section data as precise as from a point-wise activation measurements with well-defined mono-energetic neutron beams. However, this technique allows obtaining in a relatively simple and straightforward manner general information about the neutron excitation function, such as the shape, the threshold energy and the plateau cross-section value. This approach is very helpful to provide such data, where no or scarce experimental data exists.

3 Measurements

3.1 Material

For the irradiation 7 metal rhenium disks were used. The mass of each disk is listed in table 1. The material has a high level of purity with 99.9% of natural rhenium. All disks had an identical shape with a diameter of 20 mm and were 5 mm thick.

3.2 Neutron field and irradiation

The irradiation of the rhenium disks was done at the JRC-IRMM Van de Graff accelerator laboratory. For the production of the neutrons the $^3\mathrm{H}(\mathrm{d},\mathrm{n})^4\mathrm{He}$ reaction was used. The neutron-production target was a Ti–^{3}H target of 2.293 mg cm^{-2}. The ^{3}H/Ti ratio was calculated to 1.4

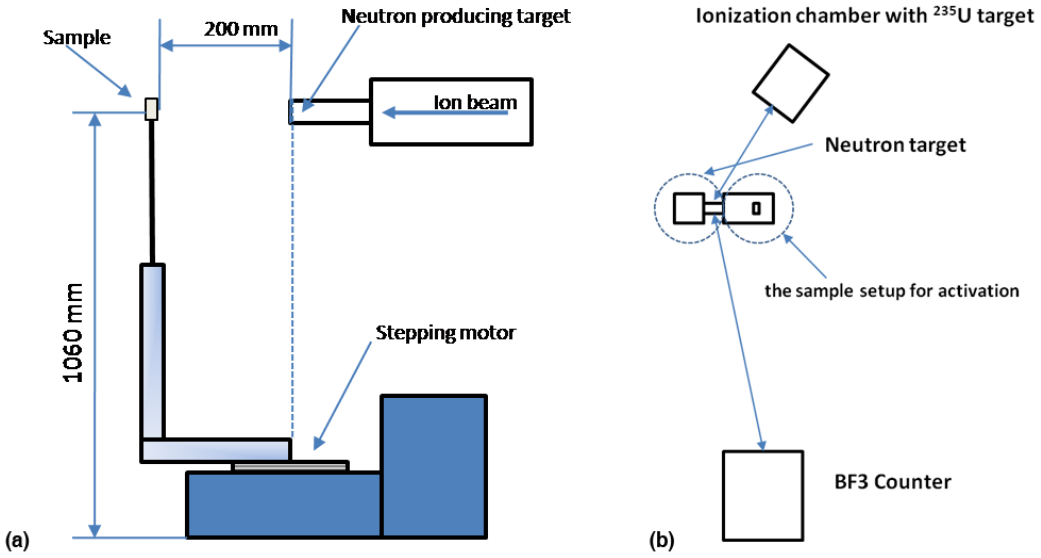

Fig. 1. (a) Schematic drawing of the sample setup for activation (not to scale). (b) Schematic drawing of the neutron fluence rate monitoring setup during an activation run (not to scale).

Table 2. Neutron irradiation data. E_i: ion energy (with uncertainty), E_n: neutron energy at 0° relative to the incident ion beam (with uncertainty) and t: irradiation time (with uncertainty).

Disk No.	E_i (MeV)	E_n (MeV)	t (s)
1	3.300(11)	19.78(20)	86921(10)
2	2.500(11)	18.71(20)	248402(10)
3	2.000(11)	18.10(28)	157632(10)
4	2.000(11)	18.10(28)	166564(10)
5	1.500(11)	17.16(30)	231958(10)
6	1.000(11)	15.97(82)	243608(10)
7	0.800(11)	15.26(131)	144831(10)

at the start of the irradiation, based on activity and production data from the manufacturer. The target had not been used before and was water-cooled during irradiation.

The critical and most important part of the NAXSUN method is the design, generation and characterization of the broad-energy overlapping neutron fields for the irradiation. 6 disks were activated by the established scanning irradiation method [15]. This means that the samples were irradiated by neutrons in front of a neutron-producing target over a certain angular interval. By scanning of the disks over different angles relative to the ion beam during irradiation, the samples were exposed to a total neutron spectrum over a broad-energy region. Each disk has been irradiated at one neutron energy and in an interval from 0° to 80° relative to the direction of the beam at 41 different positions, in steps of 2°. The irradiation time for each position was increased by one second to compensate for the decreasing flux at increasing angles. In table 2 the neutron beam energies, used for irradiation, are shown for 0° relative to the direction of the particle beam. By using 6 different beams a neutron energy range between 13 MeV and 20 MeV was covered. In addition, a seventh disk (table 2, disk No. 4) was irradiated at a fixed position at 0° at an incident neutron energy of 18.1 MeV. The obtained cross-section was used for the normalization of the excitation function, which we obtained by the unfolding technique. All disks were irradiated at a distance of 20 cm from the neutron target. For the irradiation the same setup as presented in ref. [15] was used (fig. 1(a)).

During irradiation, the neutron fluence rate was monitored by a BF_3 long counter and an ionization chamber loaded with a ^{235}U target (fig. 1(b)). Also, data about variations in the accelerator beam current was collected. These measurements were used for the normalization of the simulated neutron spectra, which are input parameters in the unfolding procedure.

The neutron spectra were simulated by means of the Monte Carlo code TARGET [20]. This code provided the neutron energy with uncertainty taking into account also the uncertainty in the ion-beam energy (cf. table 2; neutron energies are given at 0° relative to the incident ion beam together with the corresponding uncertainty). The obtained simulated values Φ_{Tj} are multiplied by the parameter b_j for experimental variations in the ion-beam current, the irradiation and cooling time [16]:

$$\Phi_j = \Phi_{Tj} \cdot b_j$$
$$b_j = \sum_{i=1}^{n} \left(\frac{q_i}{t_{aji}} \left(1 - e^{-\lambda t_{aji}}\right) e^{-\lambda t_{cji}} \right), \qquad (2)$$

where the index i indicates the summation over repeated irradiations at a certain angle, j, and n is the number of repetitions; q_i is the accumulated charge for every step; λ is the decay constant of the isotope of interest. t_{cji} is the decay time between successive irradiations for a certain angle position and t_{aji} is the time of irradiation at

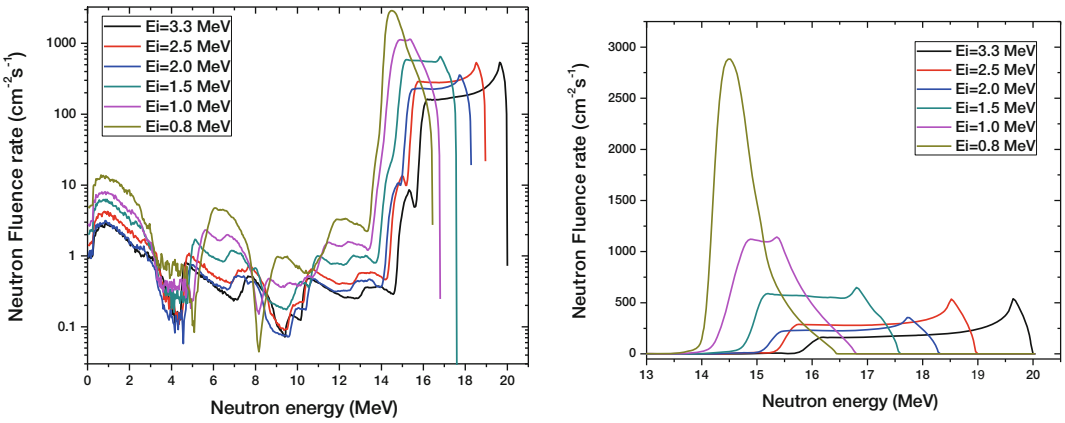

Fig. 2. Neutron fluence spectra simulated by the TARGET code, corrected by the factor b_k in case of ^{184}Ta isotopes (see text for details).

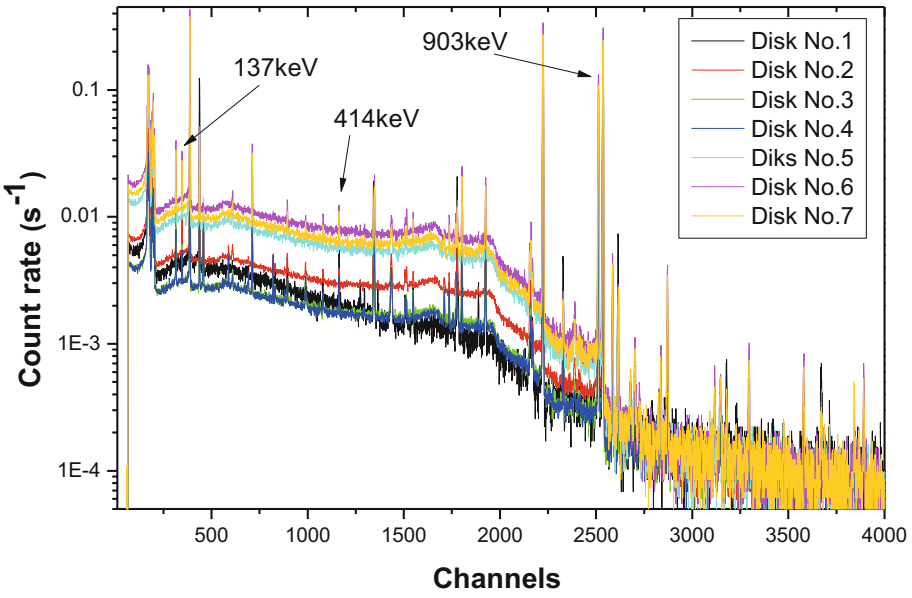

Fig. 3. Parts of detected gamma-ray spectra with the main gamma lines following the ^{187}Re(n, 2n)^{186}Re, ^{187}Re(n, α)^{184}Ta and ^{185}Re(n, 2n)^{184}Re reactions. For details about the complete gamma-ray spectrum see ref. [22].

a certain angle, j. In total irradiations at 41 different positions were performed within an interval from 0° to 80°. The obtained neutron fields used for the disk irradiations are depicted in fig. 2 in the case of the detection of ^{184}Ta from the ^{187}Re(n, α)^{184}Ta reaction.

Figure 2 shows that the neutron fields, generated by the step-wise irradiation, overlap with several other neutron spectra. This is an essential feature to insure the successful determination of neutron excitation functions by the unfolding technique. The useful neutron energy range lies between 13.08 MeV and 19.5 MeV. The neutron intensity below 13.08 MeV may be considered as negligible, because it does not contribute significantly (less than 1%) to the detected activity.

3.3 Gamma spectroscopic measurements

High-resolution gamma-ray spectroscopy was applied to the activated disks. The measurements were carried out using low-background HPGe-detectors. The first measurement of each sample started around 20 min after irradiation and was performed at JRC-IRMM using a coaxial HPGe-detector with a 40% relative efficiency. Subsequent measurements were done after 2 days in the ultra-low background underground laboratory HADES [21] using a planar point contact HPGe-detector (so-called BEGe) with 50% relative efficiency. The disks were placed in a holder with a well-defined geometry and centred on the end-cap of the HPGe-detector. In fig. 3 spectra for all activated disks, directly measured after irradiation, are presented.

The analysis of the identified gamma-rays has shown possible interferences between gamma-rays emitted from different radionuclides. The vast number of gamma-rays and interferences makes it difficult to identify and quantify all peaks in the spectrum although a comprehensive list is presented in a JRC report [22]. The most suitable gamma-ray peaks were selected being those with high yield and no

Table 3. General information about the activation reactions and corresponding values of the specific activity with reference time, *i.e.* the end of the disk irradiation.

Reaction	E_γ [keV] (I_γ)	A_k (10^{-24} Bq/atom)						
		Disk No.1	Disk No.2	Disk No.3	Disk No.4	Disk No.5	Disk No.6	Disk No.7
^{187}Re(n, 2n)^{186}Re	137.2 (9.4%)	3430(50)	9850(14)	4490(60)	4790(70)	14680(210)	26800(400)	24700(300)
^{187}Re(n, α)^{184}Ta	414.0 (73.9%)	29.10(40)	23.10(30)	16.72(23)	37.30(50)	32.00(40)	32.40(50)	31.20(40)
^{185}Re(n, 2n)^{184}Re	903 (37.9%)	334.0(50)	1315(19)	676(9)	733(10)	2250(30)	3600(50)	3260(50)

interfering peaks. Three such peaks (one per radionuclide) were chosen for the determination of the activity of ^{186}Re, ^{184}Ta and ^{184}Re (listed in table 3).

The specific activity per atom of the activated target isotope, A_k, at the end of the activation, was calculated using the formula:

$$A_k = \frac{CM}{N_a m \varepsilon P_\gamma I_A} \left(\frac{\lambda}{1 - e^{-\lambda t_m}} \right) e^{\lambda t_c}, \quad (3)$$

where C is the number of counts in a certain gamma peak, λ is the decay constant, m and M are the mass of the disk and molar mass, P_γ is the gamma-ray emission probability, I_A is the isotopic abundance, N_a is the Avogadro constant, ε is the full energy peak efficiency, t_m is the live-time of the gamma spectrometry measurement and t_c is the cooling time, which in this case was between the end of the irradiation and the start of the gamma measurement. The detection efficiency was calculated using the EGS4 Monte Carlo code [23], which also incorporated calculations of corrections for the true coincidence summing.

4 Experimental results

4.1 Cross-section values for the ^{187}Re(n, α)^{184}Ta, ^{187}Re(n, 2n)^{186}Re and ^{185}Re(n, 2n)^{184}Re reactions at 18.1 MeV neutron energy

The cross-section values for the ^{187}Re(n, α)^{184}Ta, ^{187}Re (n, 2n)^{186}Re and ^{185}Re(n, 2n)^{184}Re reactions at 18.1 MeV neutron energy are determined by measuring the induced activity and the neutron fluence rate:

$$\sigma = \frac{A_k}{\Phi_1}. \quad (4)$$

The neutron fluence rate, Φ_1 (cm^{-2} s^{-1}), is obtained as the average fluence rate corrected for variation in the ion-beam current in intervals of 10 s:

$$\Phi_1 = \Phi \cdot \sum_i^n \frac{j}{j_{avg}} \cdot \left(1 - e^{-\lambda t_{a_i}}\right) e^{-\lambda t_{c_i}}, \quad (5)$$

where j_{avg} is the average beam current throughout the time of irradiation and j is the average current for 10 s intervals. The average neutron fluence rate during irradiation is determined by the measurements with two ionization chambers with ^{238}U and ^{235}U targets. The number of

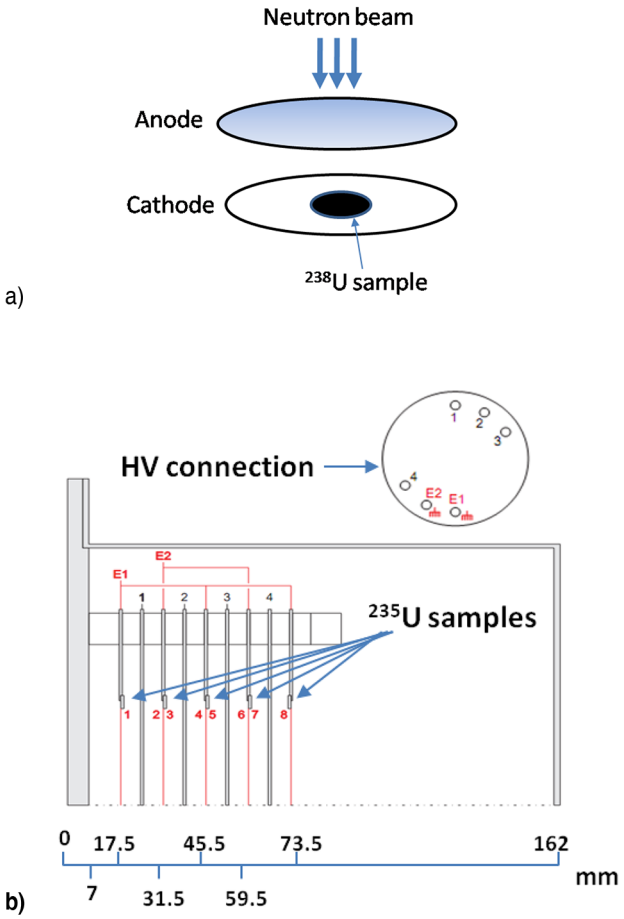

Fig. 4. (a) Drawing of the ^{238}U ionization chamber used for neutron fluence measurements; (b) technical drawing of the ^{235}U ionization chamber.

fission events, induced by neutrons in the ^{238}U and ^{235}U samples, was counted. The fission cross-section of ^{238}U is very well known and allows, therefore, determining the neutron fluence rate. The chamber with the ^{238}U target was placed at the same position as the Re disk, and the measurement was done before each disk irradiation (fig. 4). The use of fission chambers at IRMM, the data acquisition systems and details about data treatment are described in refs. [24,25].

The chamber loaded with ^{235}U was calibrated against the ^{238}U chamber and used as neutron fluence monitor during the disk activation. The chamber was, therefore,

Table 4. Incident neutron energy, average neutron fluence rate and measured cross-section for the three neutron-induced reactions on rhenium. Those values were used to normalize the neutron excitation functions.

Reaction	Neutron energy (MeV)	Φ_1 ($cm^{-2}\,s^{-1}$)	Cross section (b)
^{187}Re(n, 2n)^{186}Re	18.10(28)	6700(200)	0.713(23)
^{187}Re(n, α)^{184}Ta	18.10(28)	24600(700)	0.00152(5)
^{185}Re(n, 2n)^{184}Re	18.10(28)	811(24)	0.904(30)

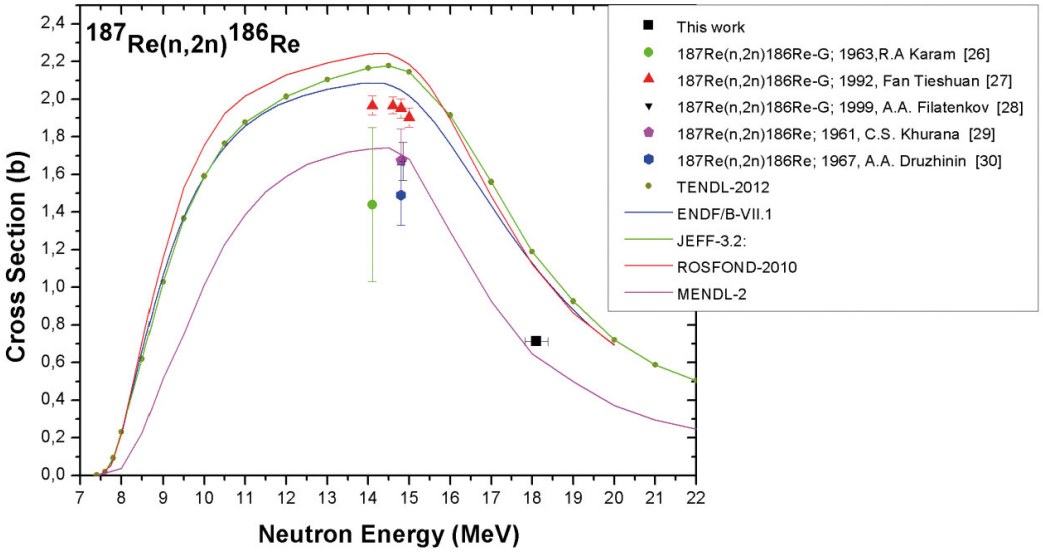

Fig. 5. Comparison of existing ENDF and EXFOR ^{187}Re(n, 2n)^{186}Re cross-section data [26–30] with our value obtained at $E_n = 18.1$ MeV.

kept at the same position, *i.e.* 111 cm away from the neutron-producing target and at 50° relative to the ion beam (fig. 1). At any moment there was a traceable link of the fission rate observed in the ^{235}U chamber with the neutron beam intensity during all disk activation runs:

$$\Phi = \frac{N_{U238}}{\sigma_{U238}} \cdot \frac{M_{U238}}{N_a \cdot m_{U238}} \cdot \frac{N_{U235\_irr}}{N_{U235\_mes}} \tag{6}$$

where m_{U238} is the mass of the ^{238}U target ($m = 0.861(16)$ mg), N_a is the Avogadro constant, σ_{U238} is the fission cross-section value of ^{238}U at the neutron energy of 18.1 MeV (from the ENDF data base 1.315(13) b). N_{U238}, N_{U235_irr}, N_{U235_mes} are given by

$$\begin{aligned} N_{U238} &= \frac{I_{U238}}{t_c} \cdot \frac{N_t}{N_e}, \\ N_{U235\_irr} &= \frac{I_{U235\_irr}}{t_c} \cdot \frac{N_t}{N_e}, \\ N_{U235\_mes} &= \frac{I_{U235\_mes}}{t_c} \cdot \frac{N_t}{N_e}, \end{aligned} \tag{7}$$

where I_{U238} and I_{U235_mes} are the detected number of fission events after fission on ^{238}U and on ^{235}U during the neutron fluence rate measurement and I_{U235_irr} is the number of fission events from fission on the ^{235}U sample during disk activation. N_t is the number of total events, which triggered the acquisition system and N_e is the total number of events processed by the acquisition system.

The obtained values for the average neutron fluence rate and cross-sections for ^{187}Re(n, α)^{184}Ta, ^{187}Re(n, 2n)^{186}Re and ^{185}Re(n, 2n)^{184}Re reactions at 18.1 MeV neutron energy, are summarized in table 4. These cross-section values are compared with existing experimental and evaluated data in figs. 5–7. In this way, the determined cross-sections were used for the normalization of the unfolded neutron excitation function, as described below. The results in figs. 5–7 show that the experimental values obtained in this work are similar to the evaluated values of MENDL-2, for ^{187}Re(n, 2n)^{186}Re and ^{185}Re(n, 2n)^{184}Re, and of EAF-2010, for ^{187}Re(n, α)^{184}Ta. Other available evaluations are off by up to 50% (cf. figs. 5 and 6).

4.2 Determination of default functions for the unfolding procedures

For the unfolding procedure, it is necessary to have a reasonable good first guess function. We determined the default cross-section function by the method described in previous NAXSUN publications [16,17]. First, the average cross-section was calculated for each irradiation in different neutron fields:

$$\langle \sigma_k \rangle \approx \frac{A_k}{\sum_i \Phi_{ki}}, \tag{8}$$

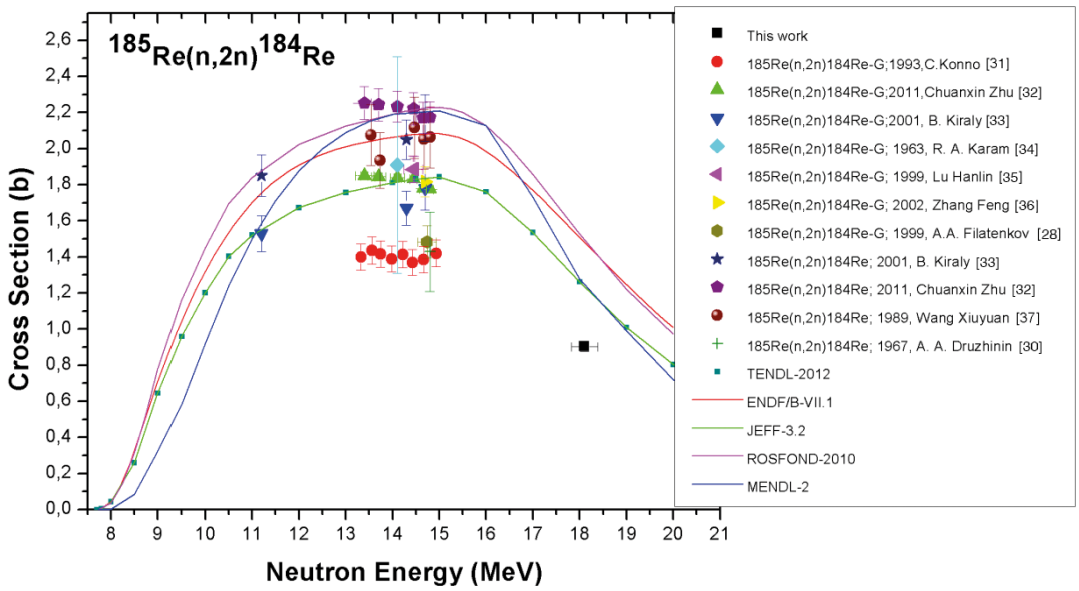

Fig. 6. Comparison of existing ENDF and EXFOR ^{185}Re(n, 2n)^{184}Re cross-section data [28,30–37] with our value obtained at $E_n = 18.1$ MeV.

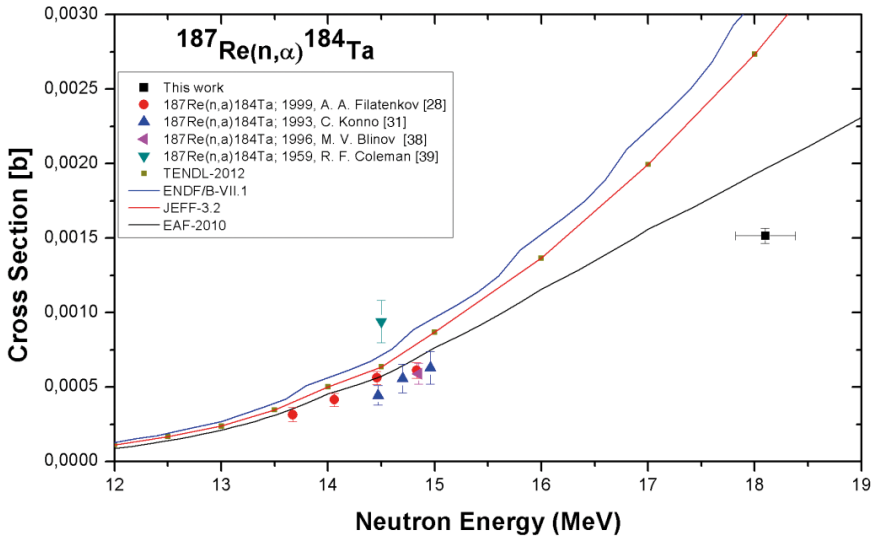

Fig. 7. Comparison of existing ENDF and EXFOR ^{187}Re(n, α)^{184}Ta cross-section data [28,31,38,39] with our value obtained at $E_n = 18.1$ MeV.

where $\langle\sigma_k\rangle$ is the average cross-section, A_k is the measured activity for disk k and Φ_{ki} is the neutron fluence for energy bin E_i.

The corresponding average neutron energies are given as

$$\langle E\rangle_k \approx \frac{\sum_i \Phi_{ki} \cdot E_i}{\sum_i \Phi_{ki}} . \quad (9)$$

The k values of the average cross-section values, which correspond to the k-th average energy, are used for the next step in obtaining the default guess function. A linear interpolation of the energy dependence of the obtained cross-section values $\langle\sigma_k\rangle$ on energy $\langle E\rangle_k$ was used. The obtained interpolated functions are normalized to the cross-section values determined for the neutron energy of 18.1 MeV. The average cross section values and determined default neutron excitation functions are listed in table 5 and presented in figs. 8–10.

4.3 Unfolding results

In this work, we used as unfolding procedures the MAXED and GRAVEL algorithms [18,19,40]. Both of them start with a guess default function defined above. The MAXED code, from all the functions, which fit the measured gamma activity (1), chooses the function that maximizes

Table 5. Average cross-section obtained from the NAXSUN scanning irradiation method.

Disk No.	$\langle E\rangle_k$ (MeV)	Φ_k ($\mathrm{cm^{-2}\,s^{-1}}$)	$\langle\sigma_k\rangle$ (b)
^{185}Re(n, 2n)^{184}Re			
1	18.3(12)	505(25)	0.90(5)
2	17.3(10)	1460(70)	1.24(6)
3	16.8(9)	740(40)	1.26(7)
5	16.1(7)	1850(90)	1.67(9)
6	15.3(6)	2300(110)	2.17(1)
7	14.7(4)	2400(120)	1.90(10)
^{187}Re(n, 2n)^{186}Re			
1	18.3(12)	4400(220)	0.71(4)
2	17.3(10)	11100(600)	0.82(4)
3	16.8(9)	6000(300)	0.69(4)
5	16.1(7)	14200(700)	0.95(5)
6	15.5(5)	17700(900)	1.39(7)
7	14.7(4)	19900(1000)	1.14(6)
^{187}Re(n, α)^{184}Ta			
1	18.3(12)	22200(1100)	0.00152(8)
2	17.3(10)	27100(1400)	0.00099(5)
3	16.8(9)	18000(900)	0.00106(6)
5	16.1(7)	34400(1700)	0.00107(6)
6	15.3(6)	41900(2100)	0.00089(5)
7	14.8(5)	68000(3000)	0.00053(3)

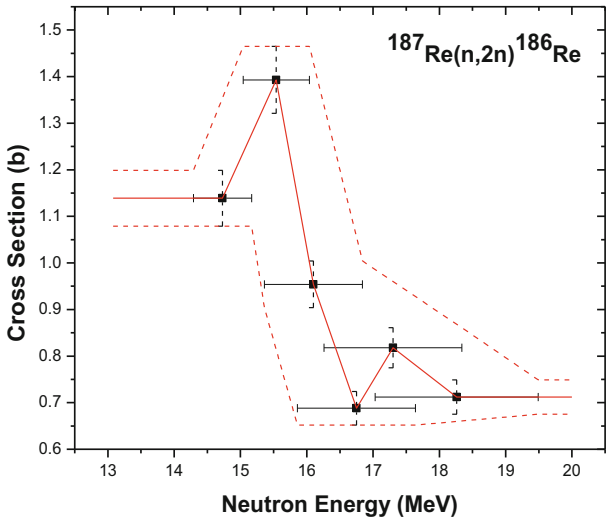

Fig. 8. Obtained default function for the ^{187}Re(n, 2n)^{186}Re reaction: the average cross-section values are given with uncertainties for the cross-section and the average neutron energy.

the relative entropy:

$$S = -\int \left\{\sigma(E)\ln\left(\frac{\sigma(E)}{\sigma_{def}(E)}\right) + \sigma_{def}(E) - \sigma(E)\right\} \mathrm{d}E, \tag{10}$$

where $\sigma_{def}(E)$ is the default cross-section function. On the other hand, GRAVEL, a slight modification of the SAND-II algorithm [19], is an iterative unfolding program:

$$\sigma_i^{J+1} = \sigma_i^J \cdot f\left(A_k, \varepsilon_k, \Phi_{ki}, \sigma_i^J\right),$$

$$f = \exp\left(\frac{\sum W_{ik}^J \log\left(\dfrac{A_k}{\sum \Phi_{ki'}\sigma_{i'}^J}\right)}{\sum_k W_{ik}^J}\right), \tag{11}$$

$$W_{ik}^J = \frac{\Phi_{ki}\cdot\sigma_i^J}{\sum_{i'}\Phi_{ki'}\sigma_{i'}^J}\frac{A_k^2}{\varepsilon_k^2},$$

where A_k is the measured activity, ε_k is the measurement uncertainty, Φ_{ki} is the neutron fluence rate for irradiation of k disk and energy bin E_i and σ_i is the cross-section for energy bin E_i.

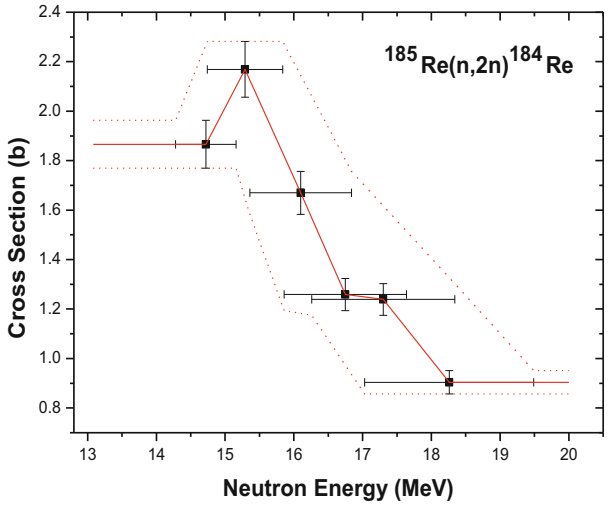

Fig. 9. Obtained default function for the ^{185}Re(n, 2n)^{184}Re reaction: the average cross-section values are given with uncertainties for the cross-section and the average neutron energy.

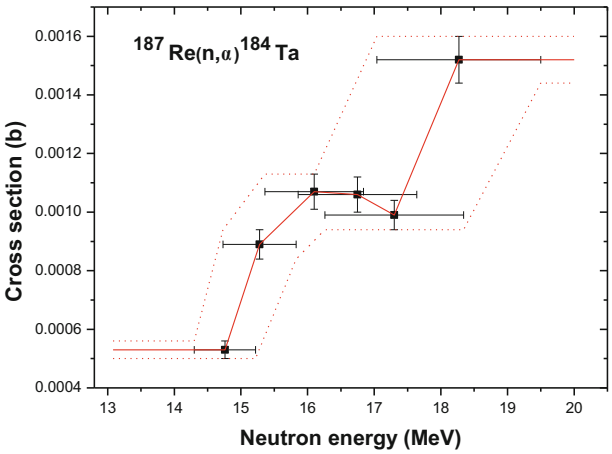

Fig. 10. Obtained default function for the ^{187}Re(n, α)^{184}Ta reaction: the average cross-section values are given with uncertainties for the cross-section and the average neutron energy.

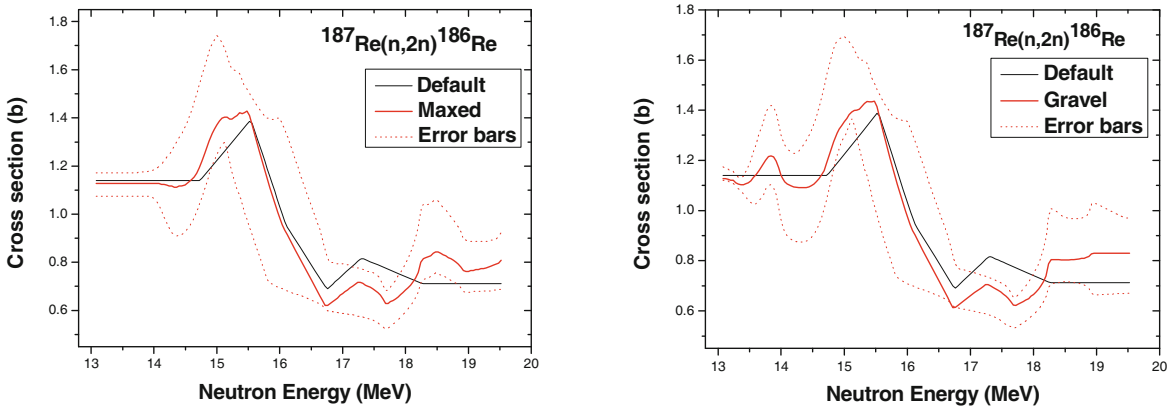

Fig. 11. Obtained unfolding function with error bars and default curve for the ^{187}Re(n, 2n)^{186}Re reaction with (a) the MAXED and (b) GRAVEL unfolding algorithms.

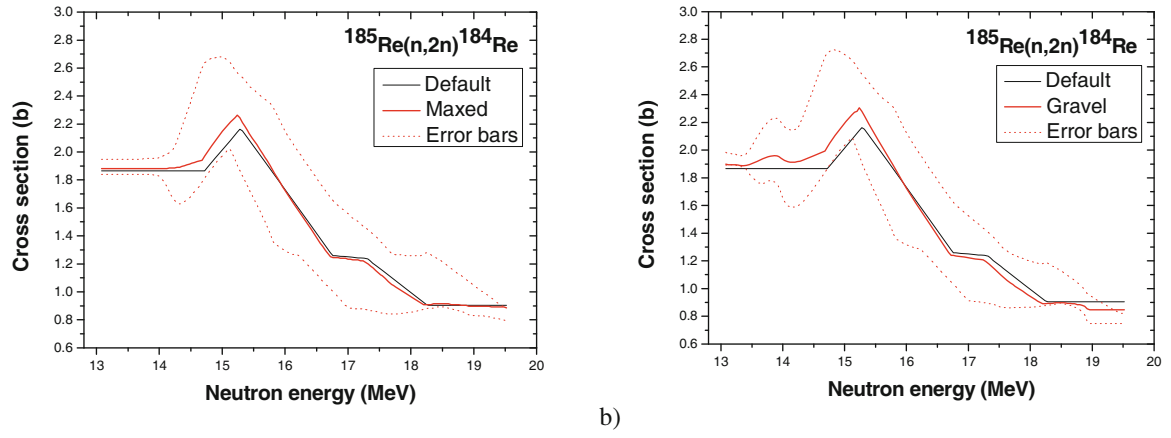

Fig. 12. Obtained unfolding function with error bars and default curve for the ^{185}Re(n, 2n)^{184}Re reaction with (a) the MAXED and (b) GRAVEL unfolding algorithms.

The unfolding was performed for 162 bins covering the range from 13.08 MeV to 19.5 MeV. The unfolding cross-section functions for the ^{187}Re(n, α)^{184}Ta, ^{187}Re (n, 2n)^{186}Re and ^{185}Re(n, 2n)^{184}Re reactions are given in figs. 11, 12 and 13, together with the default functions.

We calculated the uncertainty of the results by the unfolding procedure. This method translates the uncertainty of the default function to an uncertainty in the final cross-section function. It has been done in a way that the upper and lower error bands for the default function (see figs. 8–10) were taken as input function for the unfolding procedure. As has been mentioned in ref. [16], all sources of possible uncertainties (coming from the calculation of the neutron fields, the measurement of the induced gamma-ray activity, the measurements of the distance between the neutron-producing target and the irradiated disks, the weighting of the disks and the measurements of the beam current) contribute to the uncertainty of the determined default function and enter into the calculation of the uncertainty of the final obtained cross-section function (depicted as dashed lines in figs. 11, 12 and 13). Our analysis shows that the dominant source of uncertainty is carried by the default excitation function. This is due to the use of broad-energy neutron beams. However, obtaining the default function from a set of average cross-sections at average neutron energy assures convergence of the unfolding procedure to a stable solution. The uncertainties introduced by the width of the effective neutron fields may be large, but are carried along during unfolding. For a validation of the obtained results, an induced activity (A_c) is calculated for both, default and final cross-section function, and compared with the measured data (A_m). In table 6 we present the sum of the squared relative deviation of both values over all disks, *i.e.* the variance S, for the present three reactions:

$$S = \frac{1}{(k-1)} \sum_{1}^{k} \left(\frac{A_c - A_m}{A_m} \right)^2 . \qquad (12)$$

The results from table 6 show that the unfolding procedure converges to a better description of the measured activity data than the initial default curve.

We also compared the excitation functions obtained with the MAXED and GRAVEL codes. The results prove

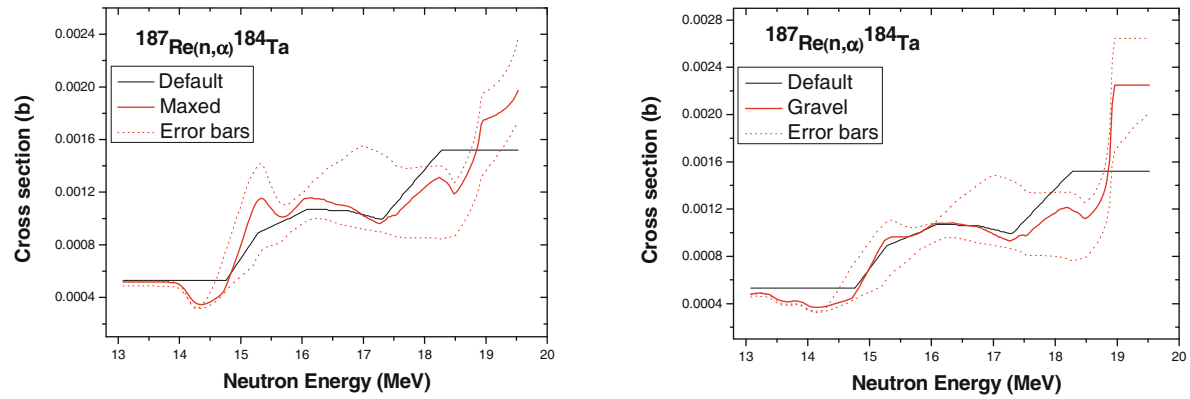

Fig. 13. Obtained unfolding function with error bars and default curve for the ^{187}Re(n, α)^{184}Ta reaction with (a) the MAXED and (b) GRAVEL unfolding algorithms.

Table 6. The sum of squares values, S, represents the relation between the measured and calculated activity.

Reaction	S		
	Default	MAXED	GRAVEL
^{187}Re(n, 2n)^{186}Re	0.021	0.013	0.013
^{185}Re(n, 2n)^{184}Re	0.0072	0.0054	0.0046
^{187}Re(n, α)^{184}Ta	0.027	0.011	0.0079

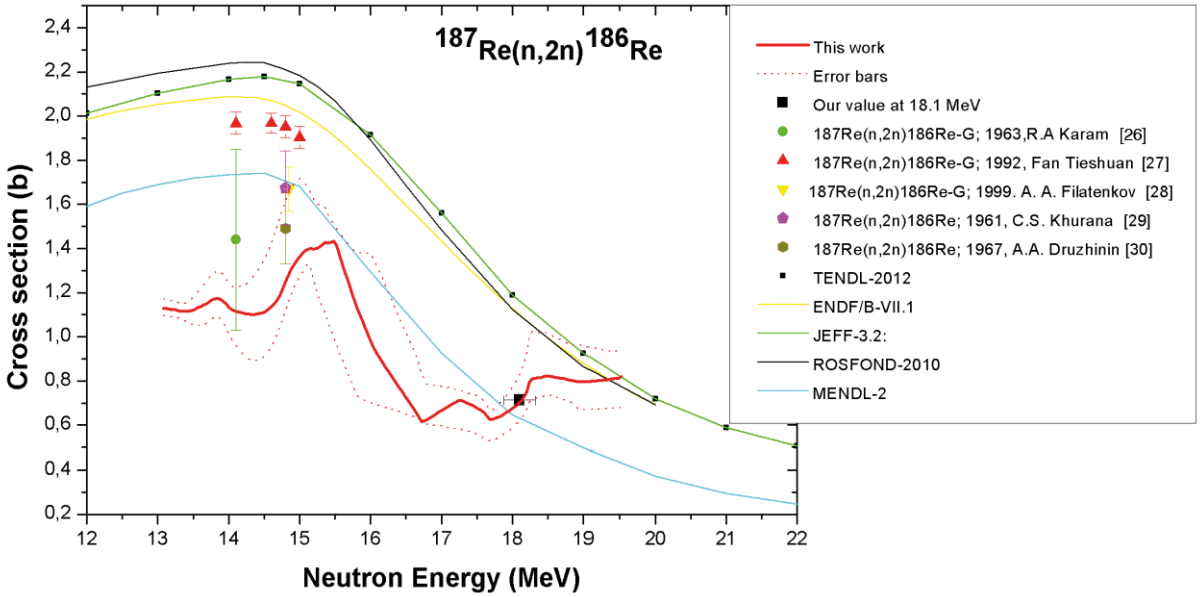

Fig. 14. Comparison of the obtained results in this work with ENDF and EXFOR data for the ^{187}Re(n, 2n)^{186}Re reaction [26–30].

that unfolding performed with the MAXED or GRAVEL code shows the same trends. The deviations between the MAXED and GRAVEL results are already reported by other authors [40]. And here again, the results can be considered as consistent within the error corridor. As the final result, the cross-sections, as average of the results from the two unfolding codes, are shown in figs. 14–16 together with the properly weighted uncertainty corridor. The results are normalized to the cross-section values determined for the neutron energy of 18.1 MeV.

In the case of ^{187}Re(n, 2n)^{186}Re, a decrease of the cross-section with increasing neutron energy is obtained. In the region around 14 MeV, the cross-section has lower values than the existing data (fig. 14). For the reaction ^{185}Re(n, 2n)^{184}Re a very good agreement with the existing data (fig. 15) is obtained. The determined cross-sec-

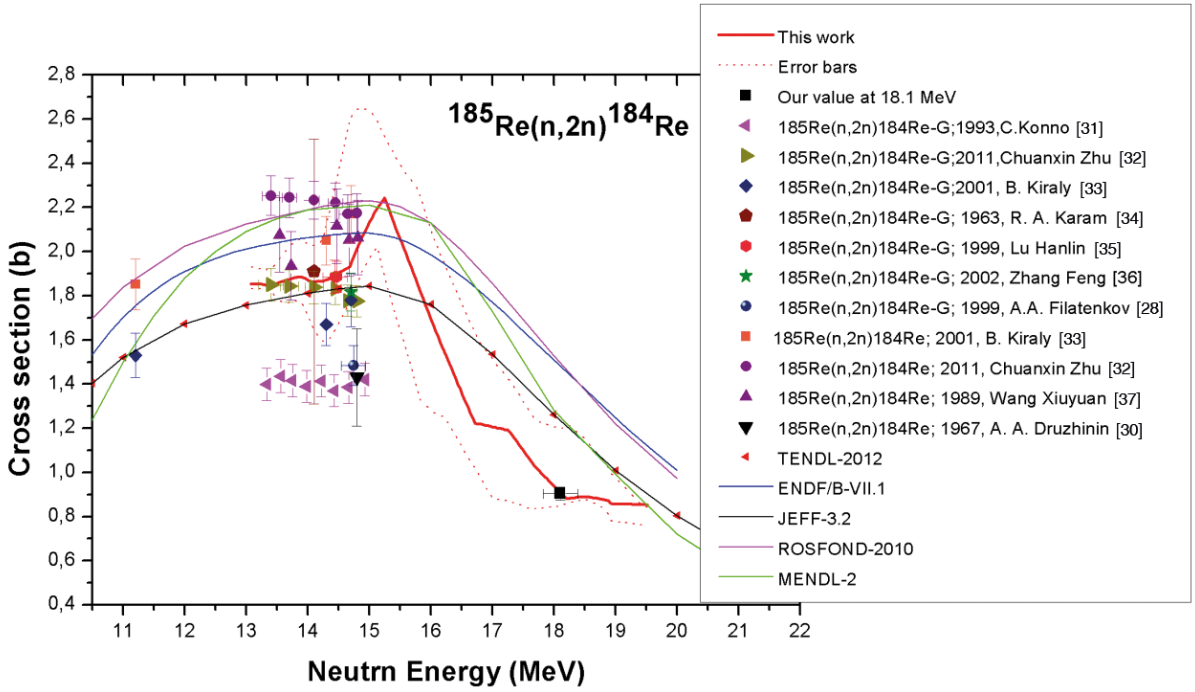

Fig. 15. Comparison of the obtained results in this work with ENDF and EXFOR data for the ^{185}Re(n, 2n)^{184}Re reaction [28, 30–37].

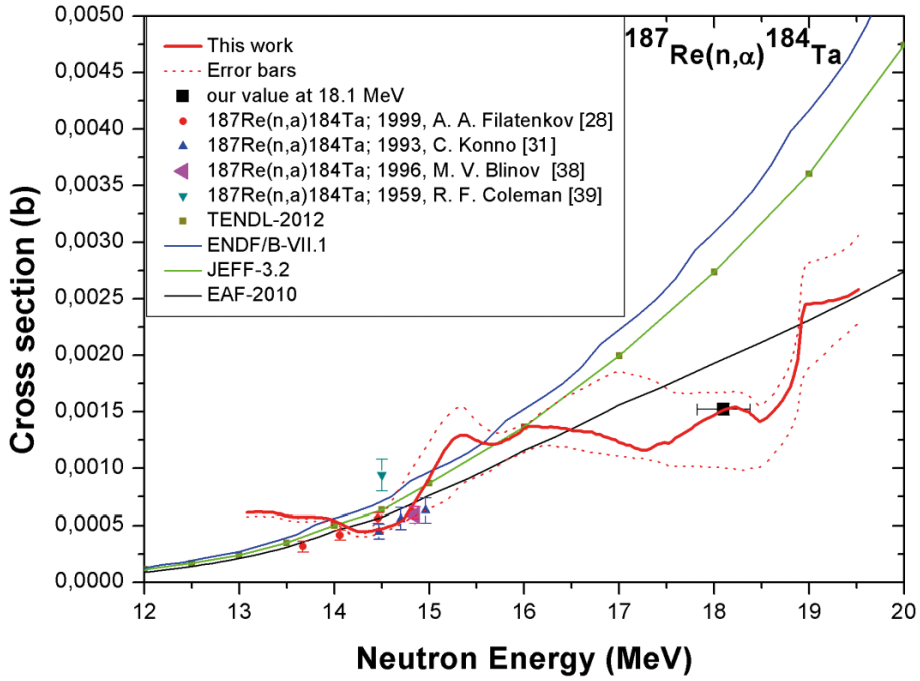

Fig. 16. Comparison of the obtained results in this work with ENDF and EXFOR data for the ^{187}Re(n, α)^{184}Ta reaction [28, 31, 38, 39].

tion function follows the trend, which is characteristic for (n,2n) reactions, showing a plateau around 14 MeV and a decreasing trend with higher neutron energy.

In both cross-sections we observe a peak-like structure around 15 MeV, which does not show in any evaluation. It is tempting to suspect a shortcoming in the fluence determination during that disk irradiation, for which we do not find evidence. However, this requires further investigation.

Figure 16 show that our neutron excitation function for the ^{187}Re(n, α)^{184}Ta reaction agrees with the existing experimental data in the region around 14.5 MeV. The function increases with neutron energy, following the evaluated data from EAF-2010.

5 Conclusions

In this work, we measured the cross-section values for the reactions ^{187}Re(n, 2n)^{186}Re, ^{185}Re(n, 2n)^{184}Re and ^{187}Re(n, α)^{184}Ta in the incident neutron energy range from 13.08 to 19.5 MeV by using the NAXSUN technique. For these reactions we present first experimental results for neutron energies between 15 and 19.5 MeV. The excitation functions were obtained by the spectrum unfolding technique and normalized by means of a dedicated cross-section measurement at incident neutron energy of 18.1 MeV. Our data show general agreement with some existing data, but are definitely ruling out others. Although the results from the ^{187}Re(n, 2n)^{186}Re and ^{185}Re(n, 2n)^{184}Re reactions do not yet allow favouring one of the present evaluations, for the ^{187}Re(n, α)^{184}Ta reaction our data are best in line with the EAF-2010 evaluation. In summary, our new data on neutron excitation functions for several rhenium isotopes may be useful to improve evaluations and nuclear models.

The activated disks will be the subject of a forthcoming study of the excitation cross-section function for the long-lived radionuclides ^{184m}Re and ^{186m}Re [41–43]. For that purpose, we will take up the gamma spectroscopic measurements of the activated disks after a time period significantly longer than the half-life of ^{184}Re and ^{186}Re.

References

1. A.B. Smith, J. Phys. G: Nucl. Part. Phys. **30**, 407 (2004).
2. P.M. Vorona, O.I. Kalchenko, V.G. Krivenko, *Neutron total cross section measurements for slow neutrons and resonance parameters of stable and radioactive isotopes* ^{185}*Re*, ^{186}*Re* ($T_{1/2} = 3.718$ *days*), in *Proceedings of the 3rd International Conference on Current Problems in Nuclear Physics and Atomic Energy, Kyiv (Ukraine), 7-12 Jun 2010*, Part II, INIS-UA–175 report (INIS Center, 2010) pp. 518–521.
3. A. Hermanne, L. Daraban, F. Tarkanyi, S. Takacs, R. Adam Rebeles, Nucl. Instrum. Methods B **267**, 3293 (2009).
4. S. Takai, G. Yamashita, K. Igawa, T. Tamyia, Tumor Res. **1**, 77 (1966).
5. Y.H. Son, G.R. Ramsby, Am. J. Roentgenol. Radium Ther. Nucl. Med. **96**, 37 (1966).
6. A. Ando, I. Ando, S. Sanada, T. Hiraki, K. Hiasada, N. Tonami, Ann. Nucl. Med. **13**, 83 (1999).
7. J. Heo, T. Htay, D. Mehta, L. Sun, J. Lacy, Nucl. Cardiol. **12**, 560 (2005).
8. D.D. Clayton, Astrophys. J. **139**, 637 (1964).
9. A.B. Smith, *Fast-Neutron Scattering from Elemental Rhenium*, Argonne National Laboratory Report ANL/NDM-155 (2003).
10. R. Macklin, P. Young, Nucl. Sci. Eng. **97**, 239 (1987).
11. A.B. Smith, P. Guenther, J. Whalen, Phys. Rev. **168**, 1344 (1968).
12. L. Cranberg, J. Levin, *Proceedings of thr Conference on Peaceful Uses of Atomic Energy (Geneva)* (United Nations Press, New York, 1955).
13. Experimental Nuclear Reaction Data (EXFOR), `https://www-nds.iaea.org/exfor/exfor.htm`.
14. The ENDF, Evaluated Nuclear Data File, `https://www-nds.iaea.org/exfor/endf.htm`.
15. G. Lövestam, M. Hult, A. Fessler, T. Gamboni, J. Gasparro, W. Geerts, R. Jaime, P. Lindahl, S. Oberstedt, H. Tagziria, Nucl. Instrum. Methods A **580**, 1400 (2007).
16. N. Jovancevic, L. Daraban, S. Oberstedt, Nucl. Instrum. Methods A **739**, 68 (2014).
17. L. Daraban, N. Jovančević, F.-J. Hambsch, M. Hult, S. Oberstedt, Phys. Proc. **59**, 138 (2014).
18. M. Reginatto, P. Goldhagen, Health Phys. **77**, 579 (1999).
19. W. Goffe, in *Studies in Nonlinear Dynamics and Econometrics*, Vol. **1**, issue No. 3 (Berkeley Electronic Press, 1996) pp. 169–176.
20. D.J. Thomas, A.V. Alevra, Nucl. Instrum. Methods A **476**, 12 (2002).
21. E. Andreotti, M. Hult, R. Gonzalez de Orduña, G. Marissens, M. Mihailescu, U. Wätjen, P. Van Marcke, *Status of underground radioactivity measurements in Hades*, in *Proceedings of the 3rd International Conference on Current Problems in Nuclear Physics and Atomic Eneregy, Kyiv (Ukraine), 7-12 June 2010*, Part II, INIS-UA–175 report (INIS Center, 2010) pp. 601–605.
22. M. Hult, H. Stroh, P. Lindahl, G. Lutter, G. Marissens, *Gamma-ray spectrometry of rhenium disks in support of neutron cross-section measurements*, JRC Technical report, in preparation (2016).
23. W.R. Nelson, H. Hirayama, D.W.O. Rogers, *The EGS4 Code System, Stanford Linear Accelerator (SLAC)* (SLAC, Stanford, CA, 1985) p. 265.
24. R. Bevilacqua, A. Göök, F.-J. Hambsch, N. Jovančević, M. Vidali, Nucl. Instrum. Methods A **770**, 64 (2015).
25. P. Salvador-Castiñeira, T. Bryś, R. Eykens, F.-J. Hambsch, A. Moens, S. Oberstedt, G. Sibbens, D. Vanleeuw, M. Vidali, Phys. Rev. C **88**, 064611 (2013).
26. R.A. Karam, T.F. Parkinson, M.F. Panczyk, *Final Technical Progress on the Nuclear Properties of Rhenium*, Department of Defence Report, No. 402668, NSR-KeyNo: 1963KA24 (1963).
27. F. Tieshuan, S. Zhaoming, T. Guoyou, L. Hanlin, Z. Wenrong, Y. Weixian, Chin. J. Nucl. Phys. **14**, 331 (1992).
28. A.A. Filatenkov *et al.*, Phys. At. Nucl. **63**, 1504 (1999).
29. C.S. Khurana, H.S. Hans, Nucl. Phys. **28**, 560 (1961).

30. A.A. Druzhinin, A.A. Lbov, L.P. Bilibin, Yad. Fiz. **5**, 18 (1967).
31. C. Konno, Y. Ikeda, K. Oishi, K. Kawade, H. Yamamoto, H. Maekawa, *Activation cross section measurements at neutron energy from* 13.3 *to* 14.9 MeV, JAERI Report, No. 1329 (1993).
32. Z. Chuanxin, C. Yuan, M. Yunfeng, Z. Pu, H. Tie, W. Xinhua, A. Li, G. Haiping, Nucl. Sci. Eng. **169**, 188 (2011).
33. B. Kiraly, J. Csikai, R. Doczi, Nucl. Sci. Eng. **129**, 164 (2001).
34. R.A. Karam, T.F. Parkinson, M.F. Panczyk, *Final technical progress report on the nuclear properties of rhenium*, Department of Defence Report, No. 402668 (1963).
35. L. Hanlin, Z. Wenrong, Y. Weixiang, H. Xiaogang, H. Xiaolong, H. Yinlu, At. En. Sci. Technol. **33**, 410 (1999).
36. Z. Feng, K. Xiang-Zhong, P. Zhong-Sheng, Z. Xue-Bin, High En. Phys. Nucl. Phys. **26**, 678 (2002) (Chinese edition).
37. W. Xiuyuan, H. Fanhua, L. Zhengtong, H. Ruiliang, *Measurements of activation cross section*, private communication with Wang (1989).
38. M.V. Blinov, A.A. Filatenkov, S.V. Chuvaev, V.A. Yakovlev, A.A. Rimskiy-Korsakov, *Systematic Measurement of Activation Cross Sections At Neutron Energies from* 13.4 *to* 14.9 MeV, IAEA Nuclear Data Section report to the I.N.D.C., No. 342 (1996) p. 53.
39. R.F. Coleman, B.E. Hawker, L.P. O'Connor, J.L. Perkin, Proc. Phys. Soc. **73**, 215 (1959).
40. R. Behrens, JINST **4**, P03027 (2009).
41. L. Hanlin *et al.*, Chin. J. Nucl. Phys. **13**, 203 (1991).
42. Y. Ikeda, C. Konno, A. Kumar, Y. Kasugai, *Summary of Activation Cross Sections Measurements At Fusion Neutron Source in JAERI*, Conference Report, IAEA Nuclear Data Section report to the I.N.D.C., No. 342 (1996) p. 19.
43. Y. Ikeda, Y. Kasugai, Y. Uno, C. Konno, H. Maekawa, *Measurements of activation cross section for* $^{187}Re(n,2n)^{186m}Re$ *and* $^{193}Ir(n,2n)^{182m2}Ir$ *at* 14 MeV *energy region*, in *Proceedings of the International Conference on Nuclear Data for Science and Technology, Gatlinburg, Tennessee, May 9–13, 1994*, Vol. **1** (American Nuclear Society, 1994) p. 1078.